Journal of Computational Applied Mechanics 2025, 56(1): 196-221

DOI: 10.22059/jcamech.2024.387317.1318

RESEARCH PAPER

Semi-analytical and numerical computations for the solution of uncertain fractional Benjamin Bona Mahony equation with triangular fuzzy number

Rambabu Vana [a], Perumandla Karunakar [a*], Snehashish Chakraverty [b]

[a] *Department of Mathematics, School of Advanced Sciences, VIT-AP University, Amaravati, India*
[b] *Department of Mathematics, National Institute of Technology, Rourkela, India*

Abstract

This manuscript introduces a semi-analytical and numerical solutions for the Benjamin Bona Mahony equation (BBME) in the form of convergent series. The BBME holds significance in diverse scientific and engineering applications. Especially to study issues on shallow water waves, solitons and their importance in modern physics. The Fuzzy Homotopy Perturbation Transform Method (FHPTM) and Differential Quadrature Method (DQM) are utilized to obtain the solutions for the BBME. In DQM, grid point based on Shifted Legendre Polynomials (SLP) have been used to solve the BBME. Additionally, we address the uncertainty in the initial condition by representing it in terms of an interval. The interval BBME (iBBME) is subsequently tackled using the FHPTM providing both lower and upper interval solutions. The convergence of the interval solution is validated considering crisp case. The outcomes obtained through FHPTM for BBME are compared with the exact solution and results obtained in this study are exhibiting good agreement. The numerical outcomes by FHPTM are compared with results obtained by DQM. Additionally, we presented the time fractional BBME and developed a fuzzy model for it, accounting for uncertainties in the coefficients associated with wave velocity. To analyze the behavior of the fuzzy time fractional BBME, and examined various numerical results using a double parametric approach.

Keywords: Fractional BBME, Fuzzy solution, FHPTM, Interval solution, Double parametric form, Shallow water waves.

1. Introduction

Research on the diverse physical structures of nonlinear partial differential equations (PDEs) has garnered significant attention due to its relevance to important scientific phenomena. The BBM equation describes long wave propagation in oceans and coastal areas, helping understand wave dynamics, the behaviour of tsunamis and aiding in

* Corresponding author. *E-mail address: karunakarperumandla@gmail.com*

hydraulic engineering for studying water wave behaviour in canals, rivers and designing structures like dams and flood and barriers. The BBME models the one-way propagation of small amplitude, long waves over shallow water surface in [1-3].

The generalized BBME (gBBME) is given by [4]

$$\frac{\partial \xi}{\partial t}+a\frac{\partial \xi}{\partial x}+\varepsilon \xi^{n}\frac{\partial \xi}{\partial x}+\theta\frac{\partial}{\partial t}\left(\frac{\partial^{2}\xi}{\partial x^{2}}\right)=0, n\geq 1,$$

where $\xi(x,t)$ symbolizes the height measured from the average water surface and x denotes the coordinate that moves the velocity of a linearized wave. ε,θ and a are constants, and n is the nonlinearity parameter. This equation generalizes the classical BBME and is widely studied for its ability to describe nonlinear dispersive wave phenomena.

In this study, we aim to reduce the gBBME to the specific form as follows [1, 5]

$$\frac{\partial \xi}{\partial t}+\varepsilon\xi\frac{\partial \xi}{\partial x}+\theta\left(\frac{\partial^{3}\xi}{\partial x^{3}}\right)=0, \tag{1}$$

which corresponds to a particular case of the gBBME with specific choices for the parameters ε,θ, $a=0$ and $n=1$. To achieve this, we analyze the coefficients of the nonlinear term $\varepsilon\,\xi^{n}\frac{\partial \xi}{\partial x}$ and compare them with the desired structure $\varepsilon\xi\frac{\partial \xi}{\partial x}$. The term $\frac{\partial \xi}{\partial x}$ in the gBBME does not appear in the target equation. To achieve this, set the coefficient of $\frac{\partial \xi}{\partial x}$ to zero, and $\theta\frac{\partial}{\partial t}\left(\frac{\partial^{2}\xi}{\partial x^{2}}\right)$ is reducing it to $\theta\left(\frac{\partial^{3}\xi}{\partial x^{3}}\right)$. This equation is a specific case of the gBBME and is notable for its role in describing nonlinear wave dynamics with a cubic nonlinearity.

As such, He's semi-inverse technique is employed to formulate the solution of generalized BBME to obtain solitary solution in [1]. The BBME with boundary condition solved using a semi discrete approach, combined with the energy method in [3]. This approach helps establish the existence and uniqueness of solutions for such a problem. Wadati [5] introduced the BBME characterizes the one-way movement of small amplitude long waves on the surface of water in a channel. It is posited as an alternative to the Korteweg–de-Vries (KdV) equation. Wazwaz [6] focused on examining the physical structures of nonlinear dispersive versions of the BBME using the sin-cosine ansatz and the analysis reveals that these generalized forms yield various solutions including compactions, soliton patterns and plane periodic solutions. Micu [7] explored the boundary controllability characteristics of the linearized BBME. It is observed to be approximately controllable but lacks spectral controllability and a finite-controllability results and provide estimates for the norms of controls required in this case. Congy et al. [8] studied an asymptotic method to explore the prolonged dynamics of the smoothed step initial value problem or the dispersive Riemann problem associated with the BBME. Gavrilyuk et al. [9] presented a comprehensive investigation of the modulations linked to the BBME. In particular, the study discerns the boundary that distinguishes the hyperbolic and elliptic regions of the modulation equations. Johnson [10] investigated the stability of a four-parameter family of spatially periodic traveling wave solution of the generalized BBME under two types of perturbations. Ankur and Jiwari [11]

investigated new soliton solutions for the generalized BBME using the tanh-coth and exp-function methods. They then truncated the infinite domain to a finite interval and developed a Galerkin finite element algorithm to simulate the model. The factorization technique was used to analyze a specific class of traveling wave solutions of the generalized BBME in [12]. The solitary wave interactions are examined through the application of conserved quantities of BBME, as detailed in [13]. The factorization approach was applied to obtain solutions for BBME in [14]. Wazwaz and Helal [15] investigated nonlinear variants of the BBME, employing the tanh method and sine–cosine method to derive a range of exact traveling wave solutions.

The BBM equation has been previously solved successfully by many authors using various techniques in the crisp case. The FHPTM and DQM methods also addresses the crisp case The FHPTM deals with uncertain cases. It is worth noting that coefficients related to initial conditions may not always be crisp numbers, as they depend on velocity, which can have associated uncertain values. To tackle this, one can substitute these crisp numbers with intervals and triangular fuzzy numbers (TFN) to establish specific bounds. The BBME into iBBME can be effectively solved using the HPTM method, which often outperforms other semi-analytical methods in terms of accuracy and efficiency.

This article provides the solution of BBM equation using HPTM. In this regard we review few works related homotopy methods which addressed nonlinear PDEs to show the effectiveness of HPTM. Karunakar and Chakravarty [16] focused on utilizing the HPTM to derive a convergent series-type solution for the fractional KdV equation. In [17], the HPTM was applied to determine interval bounds for the interval-modified Kawahara differential equation. Rambabu and Karunakar [18] examined solutions for both the regularized long-wave equation and its modified version using HPTM, focusing on both crisp and uncertain scenarios to analyze the dynamics of shallow water waves. In [19], they explored the solutions for the BBME, utilizing the HPTM to handle uncertainties in initial conditions by using interval representations for solving the iBBME.

2. Preliminaries:

nterval arithmetic operations:

An interval is defined as a subset of the real numbers $\mathbb{R}$ such that $[Z_L, Z_U] = \{t / Z_L \le t \le Z_U; Z_L, Z_L \in \mathbb{R}\}$

If $[i_1, i_2], [j_1, j_2]\, [i_1, i_2], [j_1, j_2]$ be the intervals, the arithmetic operations are as follows [20-22]:

$$[i_1, i_2] + [j_1, j_2] = [i_1 + j_1, i_2 + j_2]\, [i_1, i_2] + [j_1, j_2] = [j_1 + i_1, i_2 + j_2]$$

$$[i_1, i_2] - [j_1, j_2] = [i_1 - j_2, i_2 - j_1]\, [i_1, i_2] - [j_1, j_2] = [i_1 - j_2, i_2 - j_1]$$

$$[i_1, i_2].[j_1, j_2] = \begin{cases} [i_1 j_1,\ i_2 j_2], & \text{if } i_1, j_1 \ge 0 \\ [i_2 j_2,\ i_1 j_1], & \text{if } i_2, j_2 \le 0 \\ \left[\min\{i_1 j_2,\ i_2 j_1\}, \max\{i_1 j_2,\ i_2 j_1\}\right], & \text{Otherwise} \end{cases}$$

$$[i_1, i_2] \cdot [j_1, j_2] = \begin{cases} [i_1 j_1, i_2 j_2], & \text{for } i_1 \ge 0,\ j_1 \ge 0 \\ [i_2 j_2, i_1 j_1], & \text{for } i_2 < 0,\ j_2 < 0 \\ [min\{i_1 j_2, i_2 j_1\}, max\{i_1 j_2, i_2 j_1\}], & \text{for } i_1 i_2 \ge 0,\ j_2 \ge 0 \\ [min\{i_1 j_2, i_2 j_1\}, max\{i_1 j_2, j_2 j_1\}], & \text{for } i_1 i_2 < 0,\ j_1 j_2 < 0 \end{cases}$$

$$\frac{1}{[i_1,\, i_2]}=\begin{cases}\left[\dfrac{1}{i_1},\dfrac{1}{i_2}\right], & if\ 0\notin[i_1,i_2]\\ \left[\dfrac{1}{i_2},\infty\right)\cup\left(-\infty,\dfrac{1}{i_1}\right], & if\ i_1<0,\ i_2>0\\ \left[\dfrac{1}{i_2},\infty\right), & if\ i_1=0,\ i_2>0\\ \left(-\infty,\dfrac{1}{i_1}\right], & if\ i_1<0,\ i_2=0\end{cases}$$

$$\frac{[i_1,\, i_2]}{[j_1,\, j_2]}=\begin{cases}\left[\dfrac{i_1}{j_1},\dfrac{i_2}{j_2}\right], & if\ \ j_1,j_2>0\\ \left[\dfrac{i_2}{j_1},\dfrac{i_1}{j_2}\right], & if\ \ j_1<0,\ i_2>0\\ \left[-\infty,\dfrac{i_2}{j_1}\right]\cup\left[\dfrac{i_1}{j_2},\infty\right], & Otherwise\end{cases}$$

$$\frac{[i_1,i_2]}{[j_1,j_2]}=\begin{cases}\left[\frac{i_1}{j_1},\frac{i_2}{j_2}\right], & if\ \ j_1>0,\ j_2>0\\ \left[\frac{i_2}{j_1},\frac{i_1}{j_2}\right], & if\ j_1<0,\ j_2<0\\ \left[-\infty,\frac{i_2}{j_1}\right]\cup\left[\frac{i_1}{j_2},\infty\right], & \text{otherwise}\end{cases}$$

Triangular fuzzy number (TFN): A fuzzy number $Z_T=\left[Z_l,\, Z_c\,,\, Z_u\right]$ is referred to as a TFN if its membership function is represented μ_{Z_T} as follows [18, 20, 21],

$$\mu_{Z_T}=\begin{cases}\dfrac{x-Z_l}{Z_c-Z_l}, & if\ Z_l\le x\le Z_c\\ \dfrac{Z_u-x}{Z_u-Zc}, & if\ Z_c\le x\le Z_u\\ 0, & Otherwise\end{cases}$$

Single Parametric form: Any interval number of the form $Z=\left[\underline{Z},\,\overline{Z}\right]=[Z_l,\,Z_u]$ may be represented in the parametric form as [23] [24-27], $Z=\left[\underline{Z},\,\overline{Z}\right]=\overline{Z}+2\gamma\Delta Z$ where $\Delta Z=\dfrac{\overline{Z}-\underline{Z}}{2}$ and $0\le\gamma\le1$.

Doble Parametric form: Any fuzzy number of the form $V_T=\left[V_l,V_c,\,V_u\right]$ can be written in the parametric form as[20, 21] [23], $V_T=\left[\underline{V},\,\underline{V}\right]=\underline{V}+2\gamma\Delta V$, where $\underline{V}=V_l+\left(V_c-V_l\right)\alpha,\ \overline{V}=V_u+\left(V_c-V_u\right)\alpha,\ \Delta V=\dfrac{\overline{V}-\underline{V}}{2},\ \alpha,\gamma\in\left[0,1\right]$.

Riemann-Liouville (RL) fractional integral:

The Riemann-Liouville (RL) integral of fractional order $q>0$ for a function $\xi(t)\in C_{\Omega}$, $\Omega\geq -1$ is defined as follows [28],

$$D^{q}\xi(t)=\frac{1}{\Gamma(\alpha)}\int_{0}^{t}(t-\xi)^{q-1}\xi(x)d\xi$$

Caputo fractional derivative (CFD):

The CFD of a function $\xi(t)$, is defined as [28],

$$D_{t}^{q}\xi(t)=\frac{1}{\Gamma(k-q)}\int_{0}^{t}(t-\xi)^{k-q-1}\xi^{k}(x)d\xi, k-1\leq q\leq k, k\in N, t>0.$$

Laplace transform (LT):

The Laplace transform (LT) of a piecewise continuous function $\xi(t)$ defined on the interval $(0,\infty)$ $(0,\infty)$ is expressed as follows [29], $L[\xi(t)]=\int_{0}^{\infty}e^{-st}\xi(t)dt$, s s is parameter. The LT of the CFD of a function $\xi(t)$ is defined as follows,

$$L[\xi(t)]=s^{\alpha}L[\xi(t)]-\sum_{n=0}^{k-1}s^{q-1-n}\xi^{n}(t).$$

3. Description of implemented Fuzzy Homotopy Perturbation Transform Method

FHPTM is a semi analytical approach that combines the Laplace transform (LT) approach and homotopy perturbation method (HPM), which is known as Laplace FHPTM.

To illustrate the basic idea of FHPTM [18, 20, 21, 23, 27, 30, 31], we examine a generic nonlinear PDEs with the fuzzy source term as $\tilde{G}(x,t;\alpha,\gamma)$,

$$D\tilde{\xi}(x,t;\alpha,\gamma)+C\tilde{R}\tilde{\xi}(x,t;\alpha,\gamma)+\tilde{N}\tilde{\xi}(x,t;\alpha,\gamma)=\tilde{G}(x,t;\alpha,\gamma), \tag{2}$$

subject to initial conditions,

$$\tilde{\xi}(x,0;\alpha,\gamma)=\tilde{\varphi}(x;\alpha,\gamma), \frac{\partial}{\partial x}\tilde{\xi}(x,0;\alpha,\gamma)=\tilde{\eta}(x;\alpha,\gamma), \tag{3}$$

where $D=\frac{\partial^{2}}{\partial t^{2}}\left(or\frac{\partial}{\partial t}\right)$ is the linear operator, $\tilde{R}$ is the fuzzy linear operator whose order is less than that of D, $\tilde{N}$ is the fuzzy nonlinear operator.

The HPTM approach comprises two phases. Initially, LT is applied to both sides of equation (2). In the subsequent step, He's polynomials are utilized by homotopy to decompose the nonlinear component present in the given equation. The coefficients C, which are associated with the initial conditions or the given equation, are not always precise numerical values. This is because they often depend on several experimentally errors, which may introduce uncertainty or imprecision. To manage this uncertainty, the coefficient C can be replaced with intervals or TFN, allowing for the establishment of bounds using a parametric approach. Specifically, C can be represented as TFN, and by applying the α -cut technique, equation (2) can be derived.

Using the LT to both sides of equation (2) we obtain,

$$L\left[D\tilde{\xi}(x,t;\alpha,\gamma)\right]=-L\left[\left(\underline{C}+2\gamma\Delta C\right)\tilde{R}\tilde{\xi}(x,t;\alpha,\gamma)\right]-L\left[\tilde{N}\tilde{\xi}(x,t;\alpha,\gamma)\right]+L\left[\tilde{G}(x,t;\alpha,\gamma)\right].$$

Using the LT and the assuming D is of 2nd order differential operator, we get

$$\begin{aligned} L\left[\tilde{\xi}(x,t;\alpha,\gamma)\right] &= \frac{\tilde{\varphi}(x;\alpha,\gamma)}{s} + \frac{\tilde{\eta}(x;\alpha,\gamma)}{s^2} + \frac{1}{s^2} L\left[\tilde{G}(x,t;\alpha,\gamma)\right] \\ &= -\frac{1}{s^2}\left[L\left[\left(\underline{C} + 2\gamma\Delta C\right)\tilde{R}\tilde{\xi}(x,t;\alpha,\gamma)\right] + L\left[\tilde{N}\tilde{\xi}(x,t;\alpha,\gamma)\right]\right]. \end{aligned} \tag{4}$$

By using inverse LT on both sides of equation (4),

$$\tilde{\xi}(x,t;\alpha,\gamma) = \tilde{\pi}(x,t;\alpha,\gamma) - L^{-1}\left[\frac{1}{s^2}\left[L\left[\left(\underline{C} + 2\gamma\Delta C\right)\tilde{R}\tilde{\xi}(x,t;\alpha,\gamma)\right] + L\left[\tilde{N}\tilde{\xi}(x,t;\alpha,\gamma)\right]\right]\right], \tag{5}$$

here, the function $\tilde{\pi}(x,t;\alpha,\gamma)$ generated by the first three terms on the right side of (4).

Exploring the solutions with embedded parameters $p \in [0,1]$ as

$$\tilde{\xi}(x,t;\alpha,\gamma) = \sum_{r=0}^{\infty} p^r \tilde{\xi}_r(x,t;\alpha,\gamma). \tag{6}$$

Using He's polynomials, the nonlinear term

$$\tilde{N}\tilde{\xi}(x,t;\alpha,\gamma) = \sum_{r=0}^{\infty} p^r H_r(\tilde{\xi}), \tag{7}$$

where He's polynomials $H_r(\tilde{\xi})$ are given by [20, 21, 27, 32]

$$H_r(\tilde{\xi}_0, \tilde{\xi}_1, ..., \tilde{\xi}_r) = \frac{1}{r!}\left[\frac{\partial^r}{\partial x^r}\tilde{N}\left(\sum_{n=0}^{\infty} p^r \tilde{\xi}_n\right)\right]_{p=0}, r = 0,1,2,.... \tag{8}$$

For a detailed understanding of the generation of He's polynomials (8) through the HPM concept, readers are encouraged to refer to [33] and reference there in. By integrating the LT with the HPM and incorporating equation (6) and (7) into equation (5), the following expansion can be derived as

$$\sum_{r=0}^{\infty} p^r \tilde{\xi}_r(x,t;\alpha,\gamma) = \tilde{\pi}(x,t;\alpha,\gamma) - p\left(L^{-1}\left[\frac{1}{s^2}\left[L\left[\left(\underline{C} + 2\gamma\Delta C\right)\tilde{R}\sum_{r=0}^{\infty} p^r \tilde{\xi}_r(x,t;\alpha,\gamma)\right] - L\left[\sum_{r=0}^{\infty} p^r H_r(\tilde{\xi})\right]\right]\right]\right). \tag{9}$$

Comparing the coefficients of identical powers of $'p'$ on both sides of (9) yields,

$$p^0 : \tilde{\xi}_0(x,t;\alpha,\gamma) = \tilde{\pi}(x,t;\alpha,\gamma),$$

$$p^1 : \tilde{\xi}_1(x,t;\alpha,\gamma) = -L^{-1}\left[\frac{1}{s^2}\left[L\left[\left(\underline{C} + 2\gamma\Delta C\right)\tilde{R}\tilde{\xi}_0(x,t;\alpha,\gamma)\right] + L\left[H_0(\tilde{\xi})\right]\right]\right],$$

$$\vdots$$

$$p^r : \tilde{\xi}_r(x,t;\alpha,\gamma) = -L^{-1}\left[\frac{1}{s^2}\left[L\left[\left(\underline{C} + 2\gamma\Delta C\right)\tilde{R}\tilde{\xi}_{r-1}(x,t;\alpha,\gamma)\right] + L\left[H_{r-1}(\tilde{\xi})\right]\right]\right].$$

The solution of (2) is

$$\tilde{\xi}(x,t;\alpha,\gamma) = \lim_{p\to 1} \tilde{\xi}_r(x,t;\alpha,\gamma) = \tilde{\xi}_0(x,t;\alpha,\gamma) + \tilde{\xi}_1(x,t;\alpha,\gamma) + \ldots \tag{10}$$

4. Solution of the BBME:

4.1. Application of HPTM to the BBME

Consider the BBM equation (1) subject to the initial condition [1] [5]

$$\xi(x,0)=\frac{v}{2}\operatorname{sech}^2\left(\frac{\sqrt{v}}{2}x\right) \tag{11}$$

The exact solution of equation (1) is given as [1]

$$\xi(x,t)=\frac{v}{2}\operatorname{sech}^2\left(\frac{\sqrt{v}}{2}(x-vt)\right),$$

here, v denotes velocity of a linearized wave.

Applying the Laplace Transform on both sides of equation (1) we obtain

$$sL\left[\xi(x,t)\right]-\xi(x,0)=-L[6\xi\xi_x+\xi_{xxx}],$$

$$L\left[\xi(x,t)\right]=\frac{\xi(x,0)}{s}-\frac{1}{s}L[6\xi\xi_x+\xi_{xxx}]. \tag{12}$$

Using inverse LT on both sides of the equation (12) gives

$$\xi(x,t)=\xi(x,0)-L^{-1}\left[\frac{1}{s}L[6\xi\xi_x+\xi_{xxx}]\right]. \tag{13}$$

Using the HPM on equation (13), we obtain

$$\sum_{r=0}^{\infty}p^r\xi_r(x,t)=\xi(x,0)-p\left(L^{-1}\left[\frac{1}{s}L\left[6\sum_{r=0}^{\infty}p^rH_r(\xi)+\frac{\partial^3}{\partial x^3}\left(\sum_{r=0}^{\infty}p^r\xi_r(x,t)\right)\right]\right]\right). \tag{14}$$

He's polynomials $\mathcal{H}_r(\xi)$ are the several non-linear term $\xi\xi_x$ in [23, 27, 33]

$$\begin{aligned}
&p^0: H_0(\xi)=\xi_0\frac{\partial\xi_0}{\partial x},\\
&p^1: H_1(\xi)=\xi_0\frac{\partial\xi_1}{\partial x}+\xi_1\frac{\partial\xi_0}{\partial x},\\
&\vdots
\end{aligned} \tag{15}$$

A comparison of the coefficients of comparable powers of 'p' on both sides of (14) yields.

$$p^0:\xi_0(x,t)=\xi(x,0)=\frac{v}{2}\operatorname{sech}^2\left(\frac{\sqrt{v}}{2}x\right),$$

$$p^1:\xi_1(x,t)=-L^{-1}\left[\frac{1}{s}L\left[6H_0(\xi)+\frac{\partial^3}{\partial x^3}\left(\xi_0(x,t)\right)\right]\right],$$

$$=t\left(\frac{3v^{5/2}\sinh(m_7)^3}{2\cosh\left(\frac{\sqrt{v}x}{2}\right)^5}-\frac{v^{5/2}\sinh(m_7)}{\cosh\left(\frac{\sqrt{v}x}{2}\right)^3}+\frac{3v^{5/2}\sinh(m_7)}{2\cosh\left(\frac{\sqrt{v}x}{2}\right)^5}\right),$$

$$p^2:\xi_2(x,t)=-L^{-1}\left[\frac{1}{s}L\left[6H_1(\xi)+\frac{\partial^3}{\partial x^3}\left(\xi_1(x,t)\right)\right]\right]$$

$$=\frac{t^3}{2}\left(\frac{21v^4}{m_3}-\frac{17v^4}{8\cosh(m_7)^2}+\frac{231v^4\sinh(m_7)^2}{m_3}-\frac{30v^4\sinh(m_7)^2}{\sinh(m_7)^6}-\frac{525v^4\sinh(m_7)^4}{8\cosh(m_7)^6}-\frac{315v^4\sinh(m_7)^4}{m_2}\right)$$

$$+\frac{t^3}{2}\left(-\frac{315v^4\sinh(m_7)^6}{m_2}+\frac{3v\left(\frac{v^3}{2\cosh(m_7)^2}-\frac{3v^3}{m_5}-\frac{m_1}{m_5}+\frac{m_1}{m_4}+\frac{15v^3\sinh(m_7)^4}{m_4}\right)}{\cosh(m_7)^2}\right)$$

$$+\frac{t^3}{2}\left(\frac{3v^{3/2}\sinh(m_7)\left(\frac{3v^{5/2}\sinh(m_7)^3}{m_6}-\frac{v^{5/2}\sinh(m_7)}{\cosh(m_7)^3}+\frac{3v^{5/2}\sinh(m_7)}{m_6}\right)}{\cosh(m_7)^2}\right)$$

where $m_1=15v^3\sinh(m_7)^2, m_2=8\cosh(m_7)^8,\ m_3=8\cosh(m_7)^4,$

$m_4=4\cosh(m_7)^6,\ m_5=4\cosh(m_7)^4,\ m_6=5\cosh(m_7)^5,\ m_7=\frac{\sqrt{v}x}{2}.$

The solution of the BBME (1) as p is approximating to 1 is

$$\xi(x,t)=\lim_{p\to 1}\xi_r(x,t)=\xi_0(x,t)+\xi_1(x,t)+\ldots \tag{16}$$

4.2. Application of DQM to the BBME

In this section, DQM is applied to the BBME (1) at $\varepsilon=6,\theta=1$ to calculate the solutions at grid points based on SLP. Firstly, we need to represent the derivative terms as approximate sums, except for the derivatives with respect to t.

Hence, replacing $\xi_x(x_m,t)$ by $\sum_{n=1}^{N}a_{m\times n}\xi(x_n,t)$ and $\xi_{xxx}(x_m,t)$ by $\sum_{n=1}^{N}c_{m\times n}\xi(x_n,t)$ in equation (1), we get a set of ODEs,

$$\xi_t(x_m,t)+6\xi(x_m,t)\xi_x(x_m,t)+\xi_{xxx}(x_m,t)=0,$$

$$\xi_t(x_m,t)=-6\xi(x_n,t)\left(\sum_{n=1}^{N}a_{m\times n}\xi(x_n,t)\right)-\sum_{n=1}^{N}c_{m\times n}\xi(x_n,t)=0 \tag{17}$$

Subject to initial conditions,

$$\xi\left(x_m,0\right)=\frac{v}{2}\operatorname{sech}^2\left(\frac{\sqrt{v}}{2}x_m\right),m=1,2,3,\ldots \tag{18}$$

where $v=0.5$

Now, we solve the BBME with the given initial condition using the DQM for nodes $N=5,7,and\,9$.

First, the grid points x_m, $m = 1, 2, 3, \ldots 5$ are the roots of

$P_5(x_5) = 252x^5 - 630x^4 + 560x^3 - 210x^2 + 30x - 1 = 0,$ and may be obtained as

$x_1 = 0.046910, x_2 = 0.230765, x_3 = 0.5000000, x4 = 0.769235, x_5 = 0.953090.$

Next, the weighted coefficients of the derivatives found using equations (1) and (17) are follows

$$a_{5\times5} = \begin{pmatrix} -10.134081 & 15.403904 & -8.087087 & 3.920798 & -1.103533 \\ -1.920512 & -1.516706 & 4.805501 & -1.857116 & 0.488833 \\ 0.602336 & -2.870776 & 0.000000 & 2.870776 & -0.602336 \\ -0.488833 & 1.857116 & -4.805501 & 1.516706 & 1.920512 \\ 1.103533 & -3.920798 & 8.087087 & -15.403904 & 10.134081 \end{pmatrix}$$

By substituting the weighted coefficients $a_{5\times5}, c_{5\times5} = a_{5\times5} \times a_{5\times5} \times a_{5\times5}$ into equation (17) and using the fourth-order Runge-Kutta Method (RKM), we solved the system of nonlinear ODEs (17) along with initial conditions. The results are presented in the table. Next, we consider $N = 7$ to determine the solution of the BBM equation (1) using the DQM. Here, we obtain seven grid points x_m, $m = 1, 2, 3, \ldots 7$. These grid points correspond to the roots of the SLP of order 7.

$P_7(x_7) = 3432x^7 - 12012x^6 + 16632x^5 - 11550x^4 + 4200x^3 - 756x^2 + 56x - 1 = 0,$ Therefore, the nodes x_m are

$x_1 = 0.025446, x_2 = 0.129234, x_3 = 0.297077, x_4 = 0.500000, x_5 = 0.702923, x_6 = 0.870766, x_7 = 0.974554.$

Following the same procedure as described above using equations (1) and (17), we can determine the weighted coefficients $a_{7\times7}$. Substituting these weighted coefficients along with $c_{7\times7} = a_{7\times7} \times a_{7\times7} \times a_{7\times7}$ and the 7 grid points x_m into equation (17) gives a nonlinear system of ODEs. The results obtained from solving this system of ODEs using the RKM are presented in the table.

Next, the grid points $P_N(x_m)$ for $N = 9$ may be obtained by following the previously mentioned procedure as follows

$P_9(x_9) = 48620x^9 - 218790x^8 + 411840x^7 - 420420x^6 + 252252x^5 - 90090x^4 + 18480x^3 - 1980x^2 + 90x - 1 = 0,$

These grid points correspond to the roots of the SLP of order 9 are

$x_1 = 0.015919, x_2 = 0.081984, x_3 = 0.193314, x_4 = 0.337873, x_5 = 0.500000, x_6 = 0.662126,$
$x_7 = 0.806686, x_8 = 0.918016, x_9 = 0.984080.$

The weighted coefficients $a_{9\times9}$ are determined using equations (1) and (17) and substituting these coefficients along with $c_{9\times9} = a_{9\times9} \times a_{9\times9} \times a_{9\times9}$ and the 7 grid points x_m into equation (17) gives a system of ODEs is obtained and solved using the RKM, with the results presented in the table 3, 4 and 5.

5. Formulation of iBBME:

This section focuses on exploring the solution to the iBBME. Here, the initial condition (11) is treated as an interval number, acknowledging that its coefficients are influenced by several parameters that may not always be precise or fixed. This approach allows for the inclusion of uncertainty in the model, accommodating situations where the parameters may vary within specified intervals rather than being represented by exact values.

Taking the initial condition (11) as an interval number $\tilde{\xi}(x,0) = \frac{Z}{2}\operatorname{sech}^2\left(\frac{\sqrt{Z}x}{2}\right)$, $Z = [0.4, 0.6]$.

The governing BBM equation (1) can be transformed into the interval form

$$\frac{\partial}{\partial t}\left[\underline{\xi},\overline{\xi}\right]+\varepsilon\left[\underline{\xi},\overline{\xi}\right]\frac{\partial}{\partial x}\left[\underline{\xi},\overline{\xi}\right]+\theta\frac{\partial^3}{\partial x^3}\left[\underline{\xi},\overline{\xi}\right]=0. \tag{19}$$

Solving the interval PDE to determine the solution of the iBBM equation (19) is a challenging task. Numerous studies in the literature have explored the solution of interval differential equations using various numerical and semi analytical approaches as discussed in [18, 20, 21, 23, 25, 27, 34]. The following section provides a convergent solution in series form for the iBBM equation (19) by employing FHPTM and parametric approach [19, 24, 34].

6. Application of FHPTM to iBBME:

In this section, we once again utilize FHPTM to tackle the iBBME, considering the specified interval condition as the interval condition.

If $v=1$ in equation (11) then we considering the interval initial condition as

$$\tilde{\xi}(x,0)=\frac{Z}{2}\operatorname{sech}^2\left(\frac{\sqrt{Z}x}{2}\right),\ Z=[0.4,0.6], \tag{20}$$

if $v=0.5$ in equation (11) then now we considering the interval initial condition as

$$\tilde{\xi}(x,0)=\frac{Z}{2}\operatorname{sech}^2\left(\frac{\sqrt{Z}x}{2}\right),\ Z=[0.10,0.40].$$

This innovative method capabilities of interval arithmetic to address uncertainties inherent in the problem. By methodically expanding the solution with respect to a parameter that is velocity, FHPTM delivers precise approximations, surpassing the limitations of conventional method in certain scenarios. Expressing the interval initial condition (20) in parametric form as,

$$\tilde{\xi}(x,0;\gamma)=\frac{(\underline{Z}+2\gamma\Delta Z)}{2}\operatorname{sech}^2\left(\frac{\sqrt{(\underline{Z}+2\gamma\Delta Z)}x}{2}\right).$$

As mentioned earlier, upon establishing the connection to equation (14), we achieve

$$\sum_{r=0}^{\infty}p^r\tilde{\xi}_r(x,t;\gamma)=\tilde{\xi}(x,0;\gamma)-p\left(L^{-1}\left[\frac{1}{s}L\left[6\sum_{r=0}^{\infty}p^rH_r(\tilde{\xi})+\frac{\partial^3}{\partial x^3}\left(\sum_{r=0}^{\infty}p^r\tilde{\xi}_r(x,t;\gamma)\right)\right]\right]\right). \tag{21}$$

Comparing the coefficients of corresponding power of the variable 'p' on both sides of equation (21)

$$p^1:\tilde{\xi}_1(x,t;\gamma)=-L^{-1}\left[\frac{1}{s}L\left[6H_0(\tilde{\xi})+\frac{\partial^3}{\partial x^3}\left(\tilde{\xi}_0(x,t;\gamma)\right)\right]\right],$$

$$p^1:\tilde{\xi}_1(x,t;\gamma)=-L^{-1}\left[\frac{1}{s}L\left[6H_0(\tilde{\xi})+\frac{\partial^3}{\partial x^3}\left(\tilde{\xi}_0(x,t;\gamma)\right)\right]\right],$$

$$=L^{-1}\left[\frac{1}{s}L\left[6\left(\frac{(\underline{Z}+2\gamma\Delta Z)}{2}\operatorname{sech}^2\left(\frac{\sqrt{(\underline{Z}+2\gamma\Delta Z)}x}{2}\right)\frac{\partial}{\partial x}\left(\frac{(\underline{Z}+2\gamma\Delta Z)}{2}\operatorname{sech}^2\left(\frac{\sqrt{(\underline{Z}+2\gamma\Delta Z)}x}{2}\right)\right)\right)\right]\right]$$

$$+L^{-1}\left[\frac{1}{s}L\left[\frac{\partial^3}{\partial x^3}\left(\frac{(\underline{Z}+2\gamma\Delta Z)}{2}\operatorname{sech}^2\left(\frac{\sqrt{(\underline{Z}+2\gamma\Delta Z)}x}{2}\right)\right)\right]\right].$$

$$= t\left(\frac{6\sinh\left(\frac{x}{2}\right)\left(\frac{\gamma}{5}+\frac{2}{5}\right)}{\cosh\left(\frac{x}{2}\right)^5} - \frac{2\sinh\left(\frac{x}{2}\right)\left(\frac{\gamma}{5}+\frac{2}{5}\right)}{\cosh\left(\frac{x}{2}\right)^3} + \frac{3\sinh\left(\frac{x}{2}\right)^3\left(\frac{\gamma}{5}+\frac{2}{5}\right)}{\cosh\left(\frac{x}{2}\right)^5}\right)$$

$$p^2 : \tilde{\xi}_2(x,t;\gamma) = -L^{-1}\left[\frac{1}{s}L\left[6H_1(\tilde{\xi}) + \frac{\partial^3}{\partial x^3}\left(\tilde{\xi}_1(x,t;\gamma)\right)\right]\right],$$

$$= \frac{t^2}{2}\left(\frac{231m_2m_1}{8m_4} - \frac{525m_2m_1}{8m_3} + \frac{21m_1^2}{m_4} + \frac{315m_5m_1^2}{4m_7} + \frac{3m_1\left(\frac{m_1}{m_6} - \frac{3m_1^2}{m_4} + \frac{15m_2m_1^2}{m_3} - \frac{15m_2m_1}{2m_4} + \frac{15m_2m_1}{2m_3}\right)}{m_6}\right)$$

$$+ \frac{t^2}{2}\left(-\frac{17m_1}{8m_6} - \frac{60m_2m_1^2}{m_3} + \frac{315\sinh\left(\frac{x}{2}\right)^6}{8m_7} + \frac{3\sinh\left(\frac{x}{2}\right)\left(\frac{6\sinh\left(\frac{x}{2}\right)m_1^2}{m_8} - \frac{2\sinh\left(\frac{x}{2}\right)m_1}{m_9} + \frac{3\sinh\left(\frac{x}{2}\right)^3 m_1}{m_8}\right)}{m_9}\right)$$

here,

$$m_1 = \frac{\gamma}{5}+\frac{2}{5}, m_2 = \sinh\left(\frac{x}{2}\right)^2,\ m_3 = \cosh\left(\frac{x}{2}\right)^6,\ m_4 = \cosh\left(\frac{x}{2}\right)^4,\ m_5 = \sinh\left(\frac{x}{2}\right)^4,$$

$$m_6 = \cosh\left(\frac{x}{2}\right)^2,\ m_7 = \cosh\left(\frac{x}{2}\right)^8,\ m_8 = \cosh\left(\frac{x}{2}\right)^5,\ m_9 = \cosh\left(\frac{x}{2}\right).$$

The solution of the iBBME is

$$\tilde{\xi}(x,t;\gamma) = \lim_{p\to 1}\tilde{\xi}_r(x,t;\gamma) = \tilde{\xi}_0(x,t;\gamma) + \tilde{\xi}_1(x,t;\gamma) + \ldots \tag{22}$$

7. Formulation of time fractional BBME and its fuzzy model:

This section focuses on investigating the solutions to the time fractional BBME and its fuzzy counterpart. In this context, the velocity v in the initial condition (11) is considered a TFN, as its coefficient is influenced by several parameters that may not always be exact. We use the HPTM to address both the time fractional BBME and the fuzzy time fractional BBME under the given initial condition (11), where the velocity is represented as an uncertain. The time fractional BBME may be derived from equation (1).

$$D_t^q + \varepsilon\xi\frac{\partial\xi}{\partial x} + \theta\left(\frac{\partial^3\xi}{\partial x^3}\right) = 0, \tag{23}$$

where $D_t^q = \frac{\partial}{\partial t^q}$, $q \in (0,1]$ is the time fractional order of $\xi(x,t;q)$ and $q = 1$ then the initial condition is equation (20).

The fuzzy initial condition may be expressed from equation (11)

$$\tilde{\xi}(x,0)=\frac{V}{2}\operatorname{sech}^2\left(\frac{\sqrt{V}x}{2}\right),\ V=[0.5,\ 1,\ 1.5] \tag{24}$$

The governing time fractional BBME (23) can be expressed in an uncertain form as follows

$$D_t^q+\varepsilon\tilde{\xi}\frac{\partial\tilde{\xi}}{\partial x}+\theta\left(\frac{\partial^3\tilde{\xi}}{\partial x^3}\right)=0, \tag{25}$$

where $\xi(x,t;q,\alpha,\gamma)$ is fuzzy valued function. The proposed HPTM is intended to handle the uncertainty present in the problem. Using a parametric approach, the initial condition (24) can be expressed in the following parametric form

$$\tilde{\xi}(x,0;q,\alpha,\gamma)=\frac{(\underline{V}+2\gamma\Delta V)}{2}\operatorname{sech}^2\left(\frac{\sqrt{(\underline{V}+2\gamma\Delta V)}x}{2}\right), \tag{26}$$

where $\Delta V=\dfrac{\left(\bar{V}-\underline{V}\right)}{2}=\dfrac{\left(V_u-V_l\right)(1-\alpha)}{2},\ \alpha,\gamma\in[0,1]$

As discussed in the previous section, the methodology applying FHPTM to equation (25) utilizes the fuzzy initial condition provided in equation (26).

8. Numerical simulation and discussions:

8.1. Results in crisp case

This section displays the numerical outcomes of BBME (1) obtained through the HPTM utilizing data $\varepsilon=6,\ \theta=1,\ t=1$ and $v=1$. DQM utilizing data $\varepsilon=6,\ \theta=1,\ t=0.1$ and $v=0.5$.

Table 1, presents numerical results for specific values of $x,t=1$ and $v=1$ in equation (11). It is clear from Table 1 that the HPTM is efficient and closely approaching the actual solution. Additionally, it is worth mentioning that the HPTM demonstrates rapid convergence of the solution. It may be clearly seen that after the value of $x=18$, both term-wise and actual numerical results are same.

Table 1: Comparison of term-wise numerical outcomes of equation (1) at different values of $x,t=1$.

x	4th term solution of $\xi(x,t)$	5th term solution of $\xi(x,t)$	6th term solution of $\xi(x,t)$	Exact solution of $\xi(x,t)$
0	0.375000	0.380642	0.380642	0.393224
2	0.405300	0.404659	0.404486	0.393224
4	0.087407	0.087589	0.087607	0.090353
6	0.012669	0.012687	0.012688	0.013296
8	0.001731	0.001733	0.001733	0.001820
10	0.000235	0.000235	0.000235	0.000247
12	0.000032	0.000032	0.000032	0.000033
14	0.000004	0.000004	0.000004	0.000005
16	0.000001	0.000001	0.000001	0.000001
18	0	0	0	0
20	0	0	0	0

Table 2: Comparison of term-wise numerical outcomes of equation (1) at different values of $t, x = 10$

t	4th term solution of $\xi(x,t)$	5th term solution of $\xi(x,t)$	6th term solution of $\xi(x,t)$	Exact solution of $\xi(x,t)$
0	0.000090	0.000090	0.000090	0.000090
0.1	0.000099	0.000099	0.000099	0.000100
0.2	0.000110	0.000110	0.000110	0.00011
0.3	0.000120	0.000120	0.000121	0.000122
0.4	0.000130	0.000133	0.000133	0.000135
0.5	0.000141	0.000142	0.000147	0.000150
0.6	0.000155	0.000157	0.000159	0.000165
0.7	0.000170	0.000171	0.000173	0.000182
0.8	0.000186	0.000187	0.0001889	0.000202
0.9	0.000209	0.000210	0.000215	0.000223
1	0.000234	0.000236	0.000238	0.000246

From Table 2, it is observable that as the number of terms increases, the numerical results convergence towards the exact solutions for a fixed values of $x = 10$ and various time t and $v = 1$ in equation (11). As the error decreases, it becomes apparent that the solutions are converging. Table 3, 4, and 5 present the absolute errors of the BBM equation using HPTM and DQM based on SLP at different nodes ($N = 5, 7, 9$), with $v = 0.5$ and $t = 0.1$. It is evident that the errors of the BBM equation increase as x values increase for nodes $N = 5, 7, 9$ when using DQM based on SLP. A comparison between the errors of the BBM equation using DQM and HPTM approaches indicates that HPTM is more efficient and superior to DQM. Specifically, the errors of the BBM equation using HPTM decrease and nearly vanish for corresponding nodes at $N = 5, 7, 9$.

Table 3: Comparison of Absolute errors in DQM and HPTM at $t = 0.1, v = 0.5$ for 5 grid points.

x	Errors in DQM	Errors in HPTM
0.046910	0.000089	0.000006
0.230765	0.000575	0.000067
0.500000	0.002316	0.000060
0.769235	0.001915	0.000052
0.953090	0.002316	0.000043

Table 4: Comparison of Absolute errors in DQM and HPTM at $t = 0.1, v = 0.5$ for 7 grid points.

x	Errors in DQM	Errors in HPTM
0.025446	0.000011	0.000070
0.129234	0.000283	0.000070
0.297077	0.000748	0.000064
0.500000	0.001280	0.000060
0.702923	0.001764	0.000055

0.870766	0.002114	0.000048
0.974554	0.002303	0.000043

Table 5: Comparison of Absolute errors in DQM and HPTM at $t = 0.1, v = 0.5$ for 9 grid points.

x	**Errors in DQM**	**Errors in HPTM**
0.015919	0.000032	0.000070
0.081984	0.000154	0.000070
0.193314	0.000464	0.000069
0.337873	0.000859	0.000067
0.500000	0.001281	0.000060
0.662126	0.001670	0.000057
0.806686	0.001983	0.000051
0.918016	0.002199	0.000045
0.984080	0.002317	0.000042

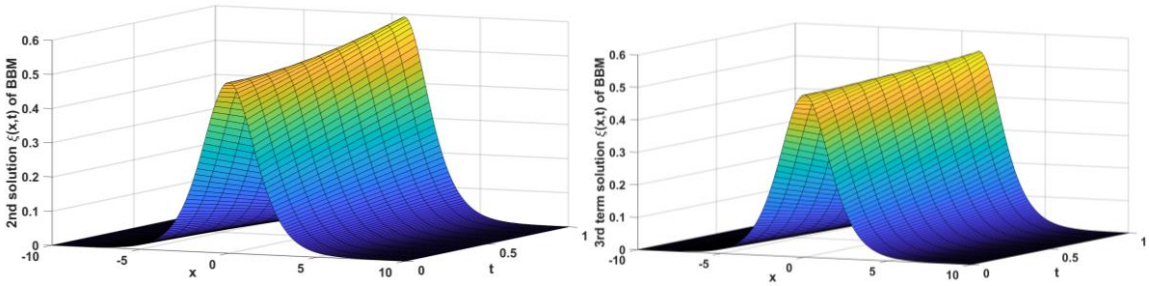

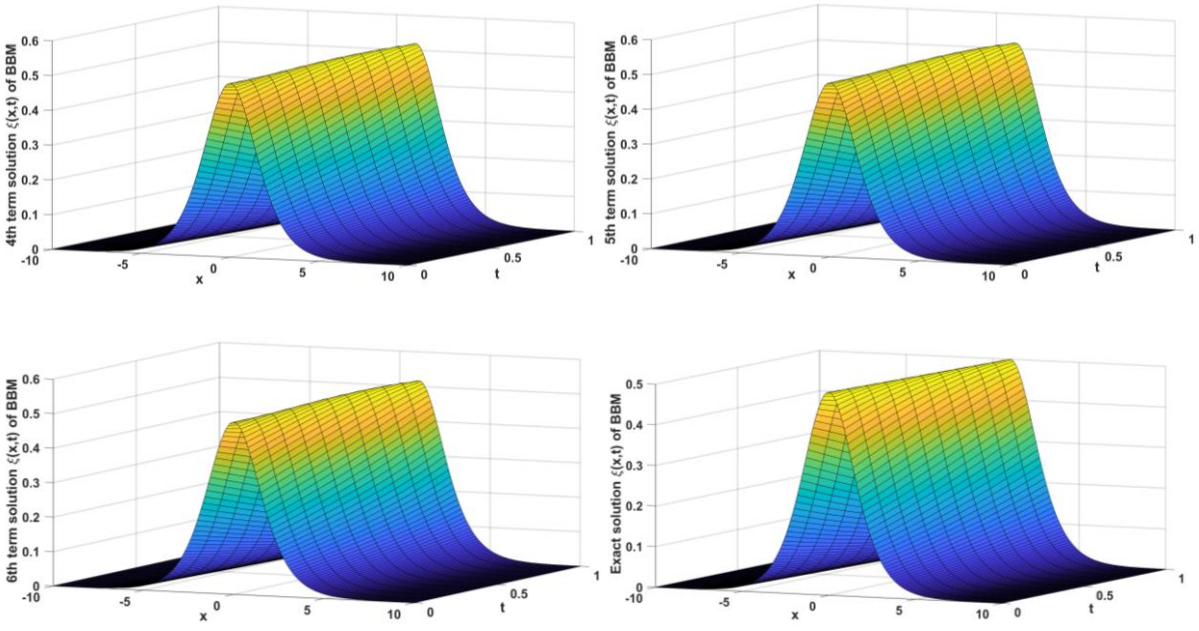

Fig. 1. Three-dimensional view of term-wise and exact solutions of equation (1).

In Fig. 1, numerical finding of the term-wise solutions and exact solution for the BBME (1) are displayed at different values of t, x and $v = 1$ in equation (11). It may be noted from the 4th, 5th, 6th term solutions and exact solutions of BBME that the water wave $\xi(x,t)$ is almost same. It is noticeable that the convergent solution of BBME is achieved as the number of terms increases. Particularly, after the 3rd term, there is no change in the wave hight. This suggest that a minimum of six terms is necessary to obtain a convergent solution for the present problem. While the required number of terms may vary for other problems but an increase in the number of terms generally leads to convergent solution. In Fig. 2, Numerical outcomes obtained from the HPTM and exact solutions for the BBME (1) are shown for various x values with $t = 0.25, 0.50, 0.75, 1$ and initial condition $v = 0.5$ in equation (11). The comparison reveals that the solution $\xi(x,t)$ obtained from the HPTM results closely matches to the exact solutions of BBME (1).

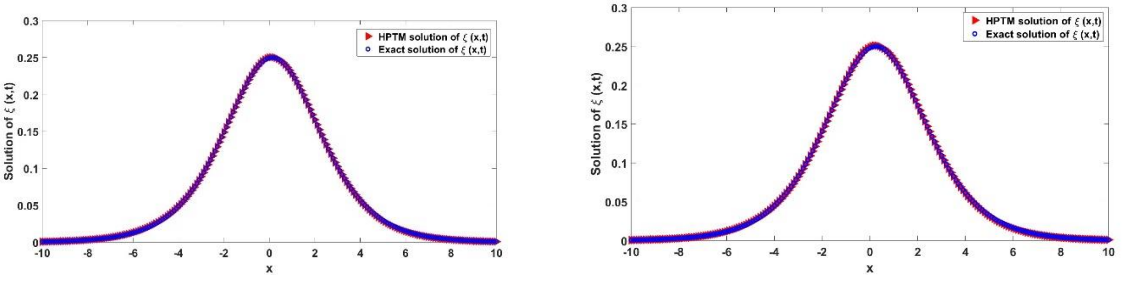

(a) at $t = 0.25$ **(b) at** $t = 0.50$

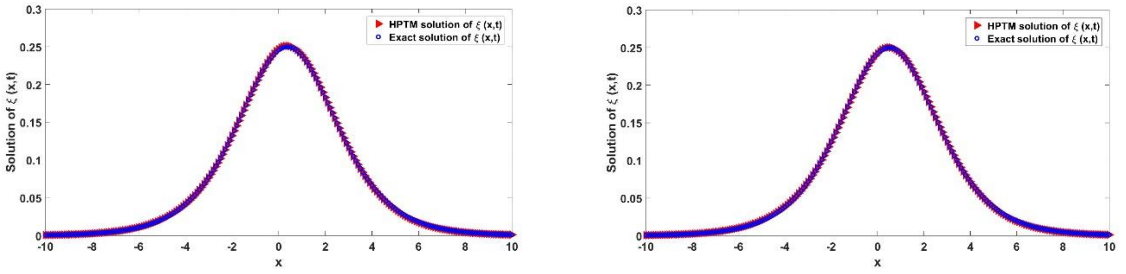

(c) at $t = 0.75$ **(d) at** $t = 1$

Fig. 2. Comparison of HPTM and exact solution of equation (1) at different time t **.**

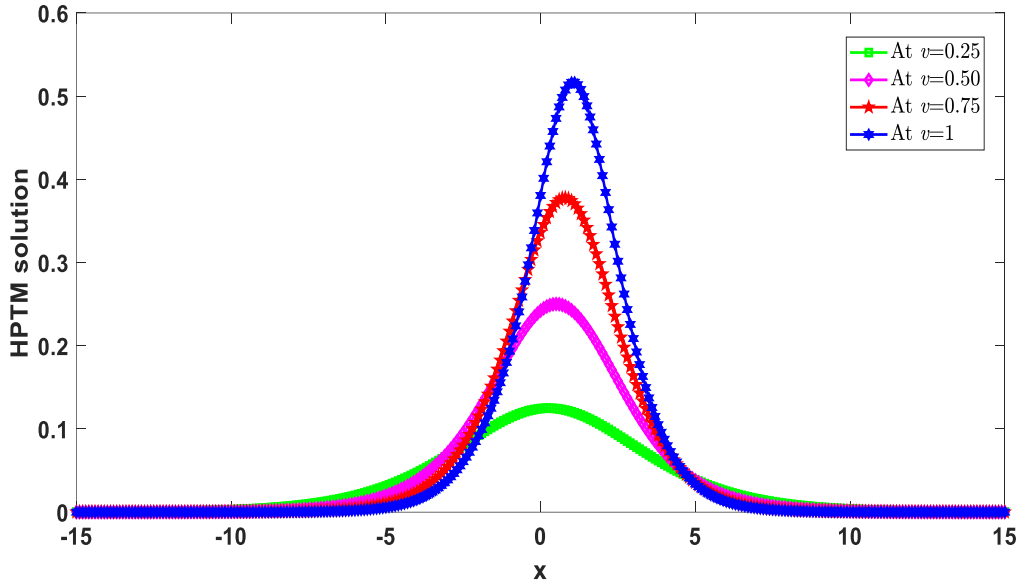

Fig. 3. HPTM solutions at different values of v

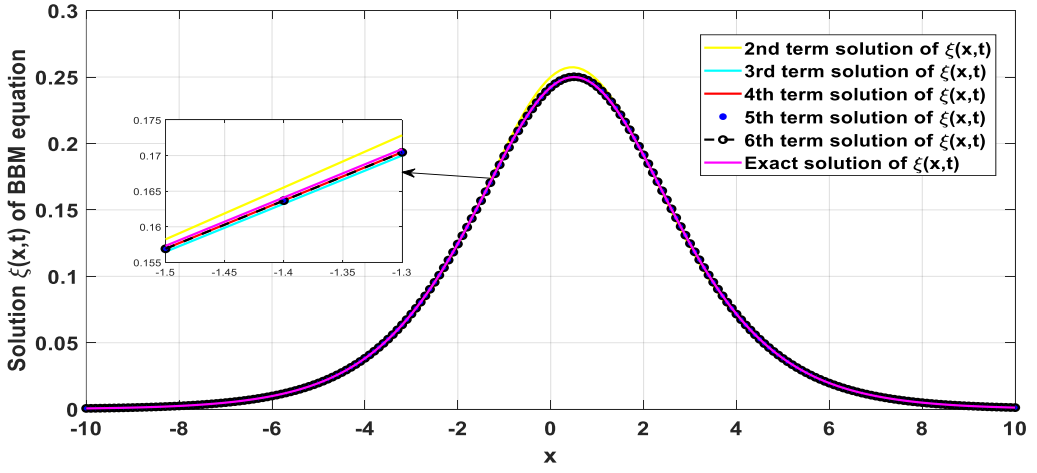

Fig. 4. Comparison of two-dimensional view of term-wise and exact solutions of $\xi(x,t)$ **.**

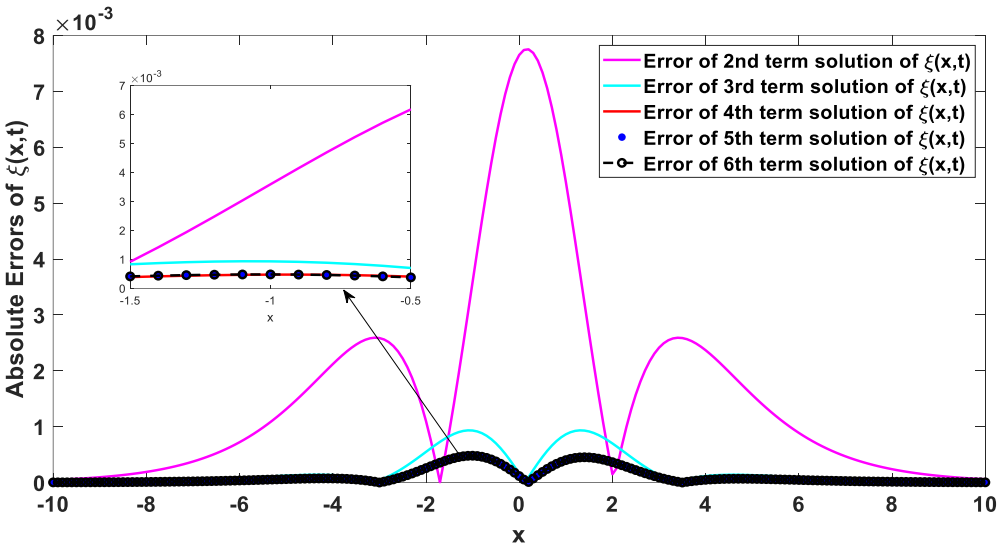

Fig. 5. Absolute errors in HPTM solution of BBME

Fig. 3 displays the HPTM solution of the BBME at different values of $v = 0.25, 0.50, 0.75, 1$. It may be observed that the peak of the solitary wave increased as the velocity (v in equation (11)) is increased. It may be clearly seen in Fig. 2 that there is no significant difference in the peak of the solitary wave as time increases for $t = 0.25, 0.50, 0.75, 1$ but the peak of the solitary wave increases with increasing velocity. Further, we generated numerical results using 2D-dimensional plots to illustrate term-wise solutions and compare these results with the actual solution. It is evident that term-wise solutions convergent to the exact solution of the BBME (1) at different values of x, $t = 1$ and $v = 0.5$ in equation (11) as shown in Fig. 4. Specifically, our numerical outcomes from the 3rd term solution to the 6th term solution closely approximate the exact solution. Consequently, the sub-plotting in Fig. 4 highlights clear results for x values from -1.5 to -1.3. Fig. 5 demonstrates that the first six terms are sufficient to achieve a convergent solution for the current BBME (1). With the increasing number of terms from first to six, the absolute error is decreases, virtually approaching zero. This illustrates the convergence, accuracy and reliability of HPTM solution (16) at $t = 1$ and $v = 0.5$ in equation (11).

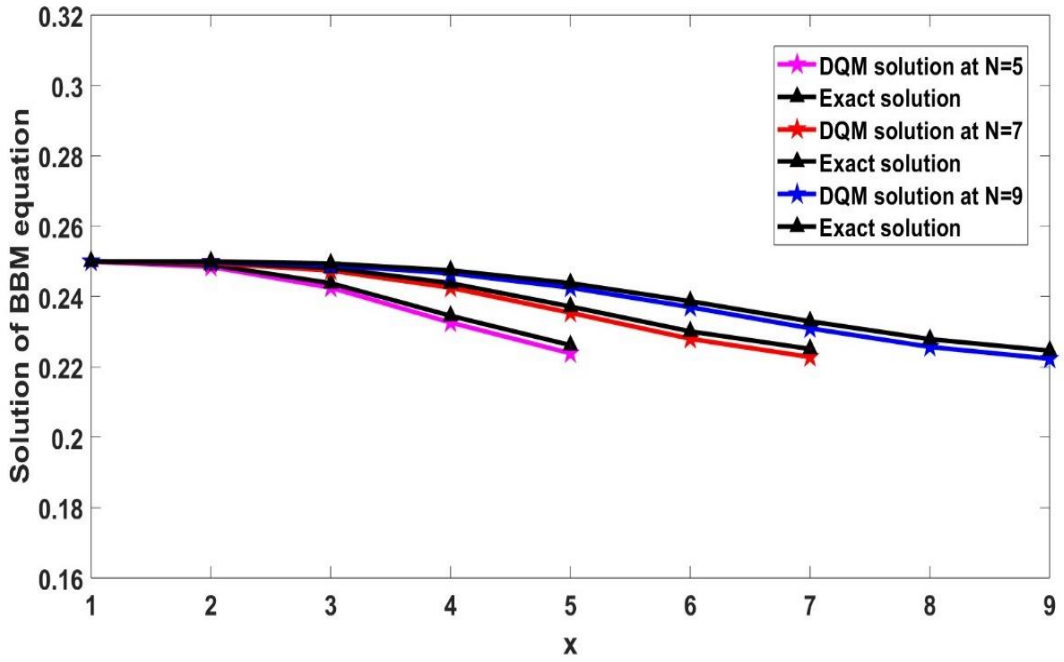

Fig. 6. Comparison of DQM and exact solutions of BBM equation

The comparison between the exact solution and the DQM solution has been computed for the nodes $N = 5, 7, 9$, the corresponding solution plots are depicted in Fig. 6. It may be noted that the DQM results closely approximate the exact solution. Fig. 7 illustrates the absolute errors in the DQM solution at nodes N=5, 7, and 9. It is evident from this figure that as the number of nodes in the DQM solution increases, the error decreases rapidly and its approaching zero.

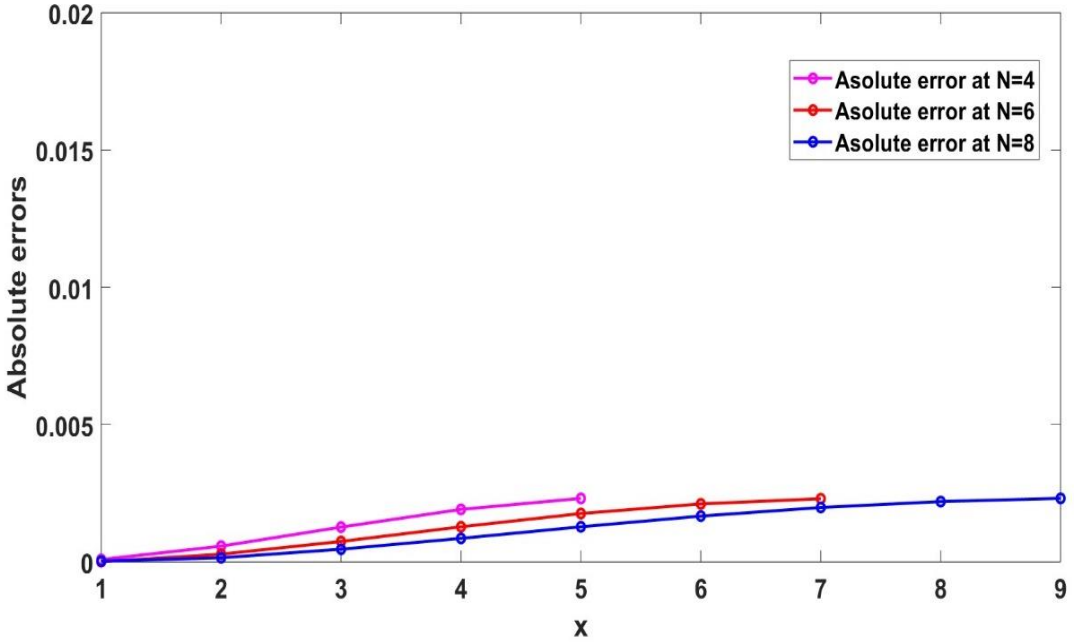

Fig. 7. Absolute errors in DQM solution of BBM equation

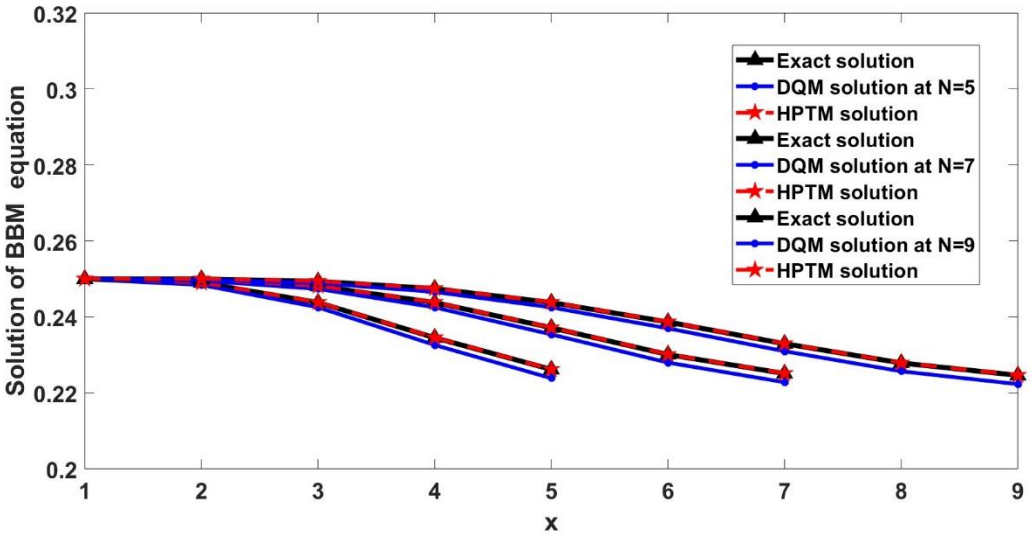

Fig. 8. Comparison between HPTM, DQM and exact solutions of BBM equation.

Fig. 8, depicts a comparison plot of the results obtained by HPTM with the numerical results from DQM based on SLP at nodes N = 5, 7, and 9. From this figure, it can be confirmed that the HPTM results exactly match the exact results of the BBME, while the DQM results only approximately match the exact solution of the BBME. From this, it may be concluded that HPTM provides better results than DQM.

8.2. Results and discussion on impressive parameters

In a similar manner, we can determine the solutions for the upper, centre and lower bounds of the interval based iBBME. The comparison results corresponding to interval solutions with the precise and crisp solution of BBME obtained when substituting $x = -10, -6, -2, 2, 6, 10$ are presented in Table 6.

Table 6. Comparison of numerical solutions of iBBME with exact solution of BBME.

x	**Lower band solution of** $\tilde{\xi}(x,t)$	**Centre solution of** $\tilde{\xi}(x,t)$	**Exact solution of** $\tilde{\xi}(x,t)$	**Crisp solution of** $\tilde{\xi}(x,t)$	**Upper band solution of** $\tilde{\xi}(x,t)$
-10	0.000030	0.000038	0.000033	0.000038	0.000045
-6	0.001680	0.002075	0.001820	0.002075	0.002462
-2	0.0111336	0.09191	0.090353	0.09191	0.219878
2	0.27065	0.404487	0.393224	0.404487	0.590921
6	0.009828	0.012689	0.013296	0.012689	0.015720
10	0.000188	0.000235	0.000246	0.000235	0.000282

Table 6, presents a comparison between numerical solutions of iBBM equation and the exact solution of BBM equation across different spatial points. For each point, lower band, center, crisp, and upper band solutions of the iBBM are given alongside the exact BBM solution, allowing for a detailed look at the iBBM's accuracy. Near the

boundaries $x=-10$ and $x=10$, all values are small and align closely with the exact solution, indicating minimal differences. Closer to the center, particularly around $x=-2$ and $x=2$, the values increase, with the upper and lower bands showing greater spread, which may indicate increased variability or non-linear behavior in the solution. Overall, this table illustrates the iBBM's accuracy across points, with the largest differences observed around $x=2.$

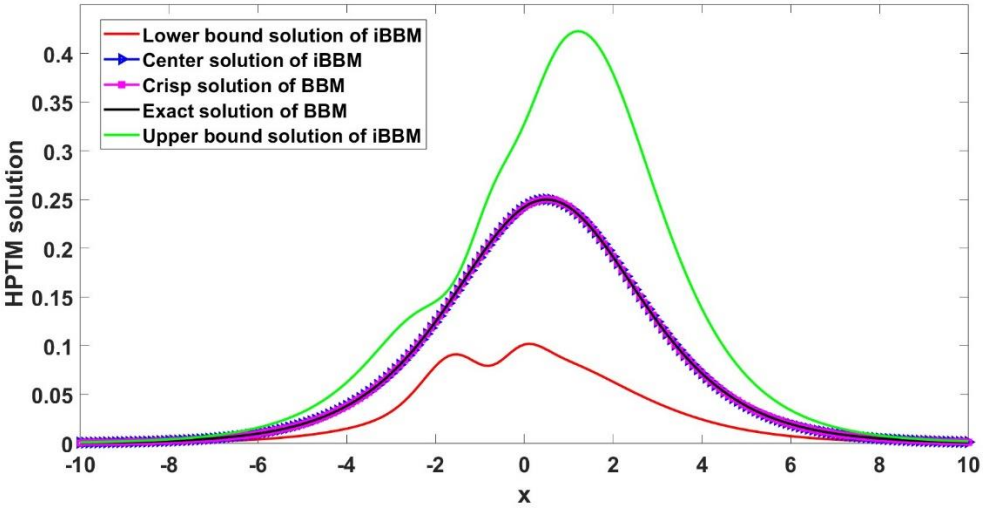

Fig. 9. Comparison of the FHPTM solution for the iBBME and BBME.

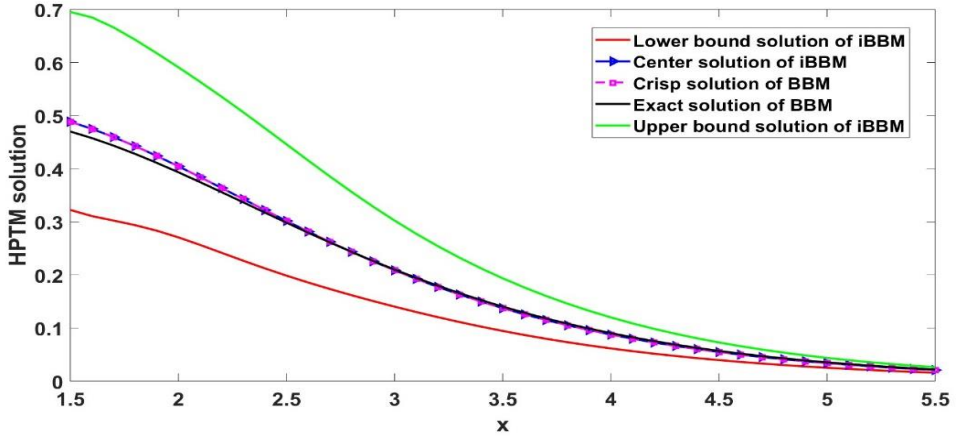

Fig. 10. Comparison of the FHPTM solution for the iBBME and BBME.

In Fig. 9, the lower, center and upper water wave elevation of the iBBME (19) are shown. These numerical findings obtained using FHPTM are compared with the actual solutions of the BBME (1) at $t=1$ and $v=0.5$ in equation (11) within the intervals $Z=[0.10,\ 0.40]$. It is clearly observed that the actual and crisp solution of BBME (1) closely approach to the center solution of iBBME (19). In Fig. 10, the lower, centre and upper water wave elevations of the iBBME (19) are depicted. These numerical outcomes by FHPTM are matching with the exact solutions of the BBME (1) at $t=1$ and $v=1$ in equation (11) and for an interval $Z=[0.4,\ 0.6]$. It is observed that the precise and accurate solution of BBME closely aligns with the centre solution of iBBME. Fig. 11, displayed the

centre solution of iBBME and the exact solutions of BBME. Notably, at various time level t, the water wave elevation ξ remains nearly same. It is observed that an increase in the wate wave height for each solution as the time t is increased.

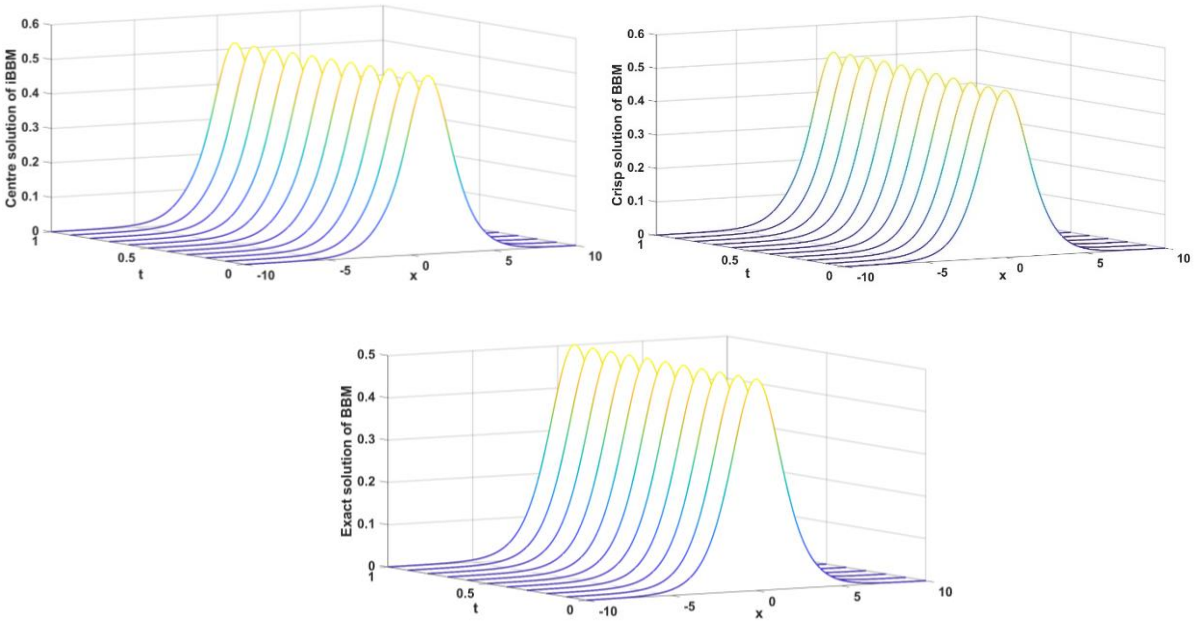

Fig. 11. Comparing the current solution and exact solution of BBME with the centre solution of iBBME.

8.3. Results and discussion on time fractional BBME and its fuzzy model

This section discusses the numerical results of the time fractional BBM equation (23) and the time fractional Fuzzy BBME (25). Equation (22) addresses the crisp case, while uncertainty in the initial condition has been considered in equation (25) as a TFN.

Table 7. Comparison of numerical solutions of BBME of different time fractional order with exact solution of BBME at $t=1$.

x	$\xi(x,t;q)$ **at** $q=0.2$	$\xi(x,t;q)$ **at** $q=0.4$	$\xi(x,t;q)$ **at** $q=0.6$	$\xi(x,t;q)$ **at** $q=0.8$	**Exact solution** $\xi(x,t;q)$
-10	-0.0001	0.0000	-0.0000	0.0000	0.0000
-8	-0.0007	0.0003	-0.0001	0.0003	0.0002
-6	-0.0049	0.0024	-0.0004	0.0021	0.0018
-4	-0.0341	0.0158	-0.0022	0.0150	0.0133
-2	-0.1599	0.0389	0.0035	0.0919	0.0904
0	0.0000	-0.1250	0.0000	0.3806	0.3932
2	0.1599	0.0389	-0.0035	0.4045	0.3932
4	0.0341	0.0158	0.0022	0.0876	0.0904
6	0.0049	0.0024	0.0004	0.0127	0.0133
8	0.0007	0.0003	0.0001	0.0017	0.0018
10	0.0001	0.0000	0.0000	0.0002	0.0002

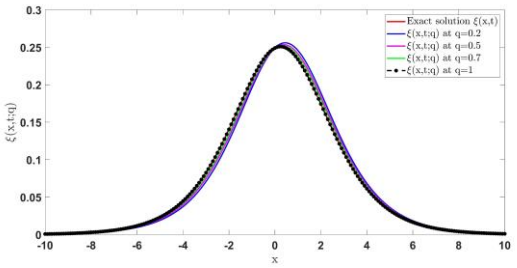

(a) $t=0.5$ and $v=0.5$

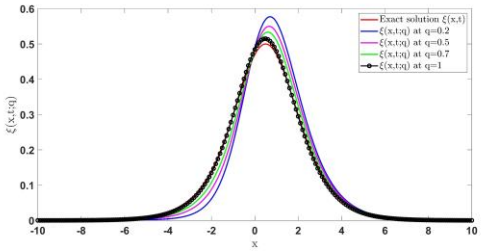

(b) $t=0.5$ and $v=1$

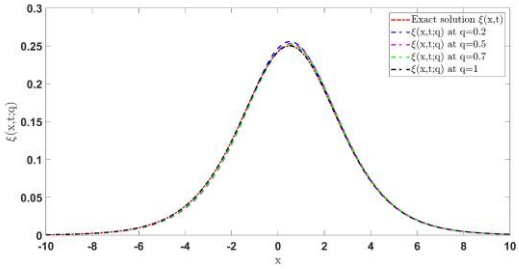

(c) $t=1$ and $v=0.5$

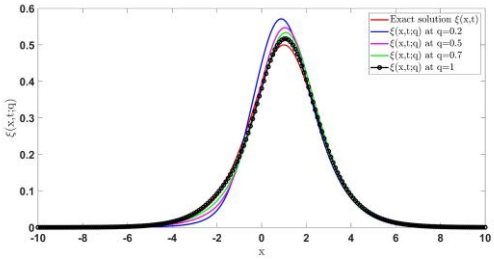

(d) $t=1$ and $v=1$

Fig. 12. Comparing the current solutions $\xi(x,t;q)$ of equation (22) and exact solution of BBME.

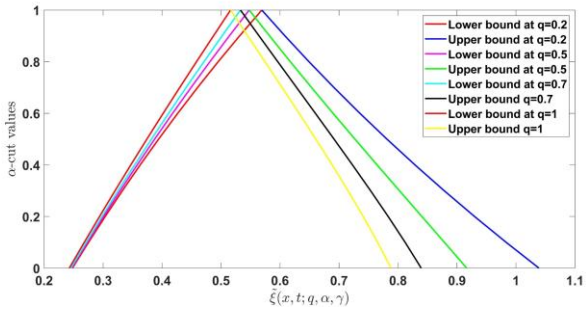

(a) $t=1$ and $x=1$

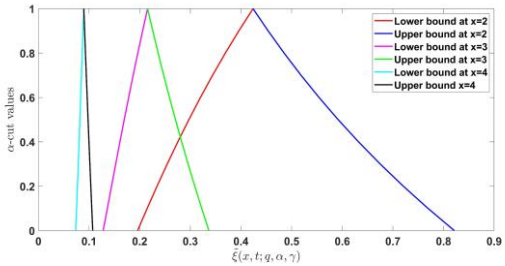

(b) $t=1$ and $q=0.5$

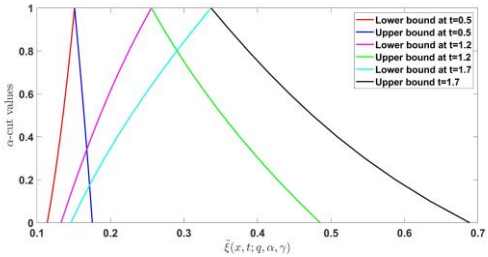

(c) $x=3$ and $q=0.7$

Fig. 13. TFN plots for FHPTM solutions $\tilde{\xi}(x,t;q,\alpha,\gamma)$ of equation (25).

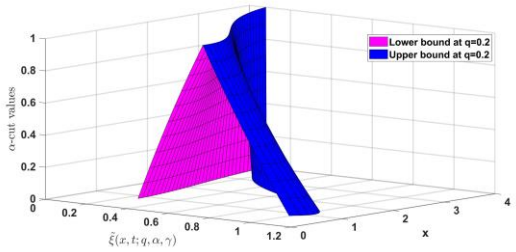

(a) $t=1$ and $q=0.2$

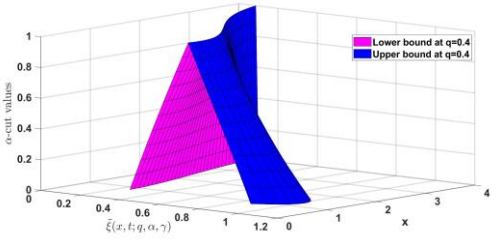

(b) $t=1$ and $q=0.4$

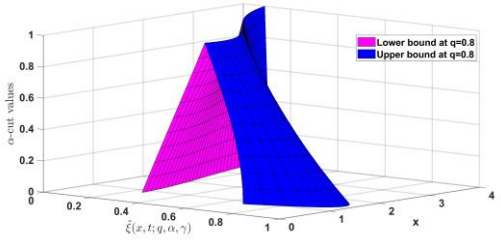

(c) $t=1$ and $q=0.8$

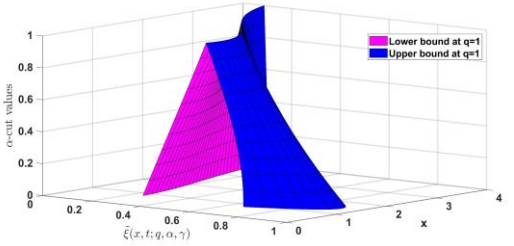

(d) $t=1$ and $q=1$

Fig. 14. 3D view of TFN plots for FHPTM solutions $\tilde{\xi}(x,t;q,\alpha,\gamma)$ of equation (25).

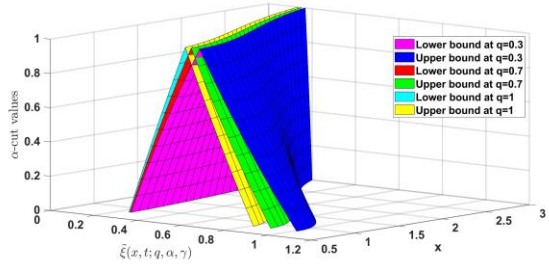

(a) $t=0.5$

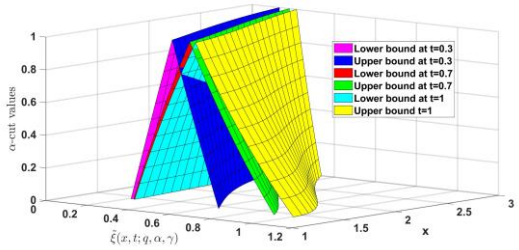

(b) $q=0.5$

Fig. 15. 3D view of TFN plots for FHPTM solutions $\tilde{\xi}(x,t;q,\alpha,\gamma)$ of equation (25).

In Table 7, we compare the numerical solutions of the BBME at different time fractional orders with the exact solution at $t=1$. Using the initial condition from equation (11) with $v=1$, the table shows the numerical solutions $\xi(x,t;q)$ for $q=0.2,0.4,0.6,0.8$ alongside the exact solution $\xi(x,t)$. At $x=-10$, the numerical solutions for $q=0.2,0.4,0.6,0.8$ and the exact solution are all close to zero, indicating minimal deviation. As x increases, the differences between the numerical solutions and the exact solution become more significant. For instance, at $x=-2$, the values for $q=0.2,0.4,0.6,0.8$ are -0.1599,0.0389,0.0035 and 0.019 respectively, while the exact solution is 0.0904. At $x=0$, the numerical solution for $q=0.6$ is -0.1250, which deviates significantly from the exact solution of 0.03932. As x increases further, the solutions gradually converge back towards the exact solution, with smaller deviations observed at $x=10$. These comparisons illustrate the impact of the fractional order q on the numerical solutions of the BBM equation. The deviations from the exact solution vary across different values of x and q, demonstrating the sensitivity of the numerical solutions to changes in the time fractional order.

Figure 12 illustrates a comparison between the numerical solutions $\xi(x,t;q)$ of the BBME (22) and the exact solution of the BBME. The figure includes results for different time fractional orders q (0.2, 0.5, 0.7, and 1) and

demonstrates how closely the numerical solutions align with the exact solution $\xi(x,t;q)$ at $t=0.5,1$. As q increases, the numerical solutions converge more closely to the exact solution, showcasing the accuracy and reliability of the proposed method for various fractional orders. The initial condition used is given in equation (20) with $v=0.5,1$.

Fig. 13 presents TFN plots for FHPTM solutions $\tilde{\xi}(x,t;q,\alpha,\gamma)$ of equation (25), showcasing how the solutions vary under different parameter conditions. In Figure 13(a), for $t=1$ and $x=1$ with varying q values (0.2,0.5,0.7 and 1), the TFNs exhibit changes in width and peak positions as q increases. Figure 13(b) illustrates the solutions for $t=1$ and $q=0.5$ with varying x values $(2, 3, \text{ and } 4)$, showing a significant decrease in the width of the TFNs and a leftward shift in their peaks as x increases. Finally, Figure 13(c) displays the TFN plots for $x=3$ and $q=0.7$ with different t values (0.5,1.2 and 1.7), where higher t values result in wider TFNs and a rightward shift in their peaks. These figures collectively illustrate the wave dynamic of the TFN solutions in response to changes in the parameters q, x and t.

Fig. 14 displays 3D views of TFN plots for the FHPTM solutions $\tilde{\xi}(x,t;q,\alpha,\gamma)$ of equation (25). These plots illustrate the behavior of fuzzy solutions at a fixed time $t=1$ with varying parameter q. Specifically, Fig. 14(a) corresponds to $q=0.2$, Fig. 14(b) to $q=0.4$, Fig. 14(c) to $q=0.8$, and Fig. 14(d) to $q=1$. In each plot, the pink surface represents the lower bound of the TFN, while the blue surface represents the upper bound. As q increases, the separation between these bound's changes, highlighting the sensitivity of the fuzzy solutions to the parameter q. These visualizations aid in understanding how q influences the fuzzy dynamics of the system described by equation (25).

Fig. 15 showcases 3D views of TFN plots for FHPTM solutions $\tilde{\xi}(x,t;q,\alpha,\gamma)$ of equation (25) and illustrates the TFN plots at $t=0.5$, highlighting the lower and upper bounds at different q values: magenta for the lower bound solution at $q=0.3$, blue for the upper bound solution at $q=0.3$, red for the lower bound at $q=0.7$, green for the upper bound solution at $q=0.7$, cyan for the lower bound solution at $q=1$, and yellow for the upper bound solution at $q=1$. In Fig. 15(b), the TFN plots at $q=0.5$ are shown, focusing on the lower and upper bounds at various t values: magenta for the lower bound solution at $t=0.3$, blue for the upper bound solution at $t=0.3$, red for the lower bound solution at $t=0.7$, green for the upper bound at $t=0.7$ cyan for the lower bound at $t=1$, and yellow for the upper bound at $t=1$. These plots visually represent the behavior of the FHPTM solutions across the specified ranges of t and q.

9. Conclusion

In this research, we effectively addressed the nonlinear BBME using a semi analytical approach, resulting in a convergent series solution. Utilizing FHPTM, we derive a series solution for the BBME. Numerical solutions of the BBME have been obtained at selected grid points using DQM based on SLP. The numerical outcomes obtained from our approach exhibit accuracy as evidenced by the figures presented. Through a comparison with

actual solution, we observed that the numerical results align well, indicating a good agreement. The obtained results confirm that the solutions of the BBME obtained by FHPTM are in good agreement with DQM results. The numerical results observed that the behaviour of the water wave forming at different velocities affects the peak height of the shallow water wave, depending on the velocity of the solitary wave. The numerical findings indicate that both methods are easy to implement, effective and reliable. Subsequently, we incorporated the initial condition coefficient within an interval framework, leading to the transformation of the BBME into iBBME. This transformation resulted leads to the iBBME. Once again FHPTM was employed to solve the iBBME. Furthermore, we have successfully presented and analyzed the time fractional BBME within the framework of a fuzzy model, addressing the uncertainties associated with wave velocity coefficients. Our approach incorporated a double parametric strategy to investigate the behavior of the fuzzy time fractional BBME.

Funding: Not applicable.

Availability of data and materials: The article contains no associated data.

Conflict of interest: The authors declare that they have no conflict of interest.

References

[1] Y.-H. Ye, L.-F. Mo, He's variational method for the Benjamin–Bona–Mahony equation and the Kawahara equation, *Computers & Mathematics with Applications,* Vol. 58, No. 11-12, pp. 2420-2422, 2009.

[2] M. Wadati, The exact solution of the modified Korteweg-de Vries equation, *Journal of the Physical Society of Japan*, Vol. 32, No. 6, pp. 1681-1681, 1972.

[3] L. Medeiros, G. P. Menzala, Existence and uniqueness for periodic solutions of the Benjamin–Bona–Mahony equation, *SIAM Journal on Mathematical Analysis,* Vol. 8, No. 5, pp. 792-799, 1977.

[4] M. A. Noor, K. I. Noor, A. Waheed, E. A. Al-Said, Some new solitonary solutions of the modified Benjamin–Bona–Mahony equation, *Computers & Mathematics with Applications,* Vol. 62, No. 4, pp. 2126-2131, 2011.

[5] M. Wadati, Introduction to solitons, *Pramana,* Vol. 57, pp. 841-847, 2001.

[6] A.-M. Wazwaz, Exact solutions with compact and noncompact structures for the one-dimensional generalized Benjamin–Bona–Mahony equation, *Communications in Nonlinear Science and Numerical Simulation,* Vol. 10, No. 8, pp. 855-867, 2005.

[7] S. Micu, On the controllability of the linearized Benjamin--Bona--Mahony equation, *SIAM Journal on Control and Optimization,* Vol. 39, No. 6, pp. 1677-1696, 2001.

[8] T. Congy, G. El, M. Hoefer, M. Shearer, Dispersive riemann problems for the benjamin–bona–mahony equation, *Studies in Applied Mathematics,* Vol. 147, No. 3, pp. 1089-1145, 2021.

[9] S. Gavrilyuk, Y. H. Lin, K. M. Shyue, Hyperbolicity study of the modulation equations for the Benjamin–Bona–Mahony equation, *Studies in Applied Mathematics,* Vol. 151, No. 2, pp. 536-554, 2023.

[10] M. A. Johnson, On the stability of periodic solutions of the generalized Benjamin–Bona–Mahony equation, *Physica D: Nonlinear Phenomena,* Vol. 239, No. 19, pp. 1892-1908, 2010.

[11] Ankur, R. Jiwari, New multiple analytic solitonary solutions and simulation of (2+ 1)-dimensional generalized Benjamin-Bona-Mahony-Burgers model, *Nonlinear Dynamics,* Vol. 111, No. 14, pp. 13297-13325, 2023.

[12] P. Estévez, Ş. Kuru, J. Negro, L. Nieto, Travelling wave solutions of the generalized Benjamin–Bona–Mahony equation, *Chaos, Solitons & Fractals,* Vol. 40, No. 4, pp. 2031-2040, 2009.

[13] X. You, H. Xu, Q. Sun, Analysis of BBM solitary wave interactions using the conserved quantities, *Chaos, Solitons & Fractals,* Vol. 155, pp. 111725, 2022.

[14] S. Kuru, Compactons and kink-like solutions of BBM-like equations by means of factorization, *Chaos, Solitons & Fractals,* Vol. 42, No. 1, pp. 626-633, 2009.

[15] A.-M. Wazwaz, M. Helal, Nonlinear variants of the BBM equation with compact and noncompact physical structures, *Chaos, Solitons & Fractals,* Vol. 26, No. 3, pp. 767-776, 2005.

[16] P. Karunakar, S. Chakraverty, Solutions of time-fractional third-and fifth-order Korteweg–de-Vries equations using homotopy perturbation transform method, *Engineering Computations*, Vol. 36, No. 7, pp. 2309-2326, 2019.

[17] P. Karunakar, S. Chakraverty, *Solution of interval-modified Kawahara differential equations using homotopy perturbation transform method*, in: *Wave Dynamics*, Eds., pp. 193-202: World Scientific, 2022.

[18] R. Vana, K. Perumandla, Uncertainties in regularized long-wave equation and its modified form: A triangular fuzzy-based approach, *Physics of Fluids*, Vol. 36, No. 4, 2024.

[19] R. Vana, K. Perumandla, Computational approach and convergence analysis for interval-based solution of the Benjamin–Bona–Mahony equation with imprecise parameters, *Engineering Computations*, 2024.

[20] R. Vana, P. Karunakar, Fuzzy uncertainty modeling of generalized Hirota–Satsuma coupled Korteweg–de Vries equation, *Physics of Fluids*, Vol. 36, No. 9, 2024.

[21] R. Vana, P. Karunakar, A fuzzy semi-analytical approach for modeling uncertainties in solitary wave solution of coupled nonlinear Boussinesq equations, *Physica Scripta*, Vol. 99, No. 10, pp. 105218, 2024.

[22] R. E. Moore, 1966, *Interval analysis*, prentice-Hall Englewood Cliffs,

[23] P. Karunakar, S. Chakraverty, T. Rao, K. Ramesh, A. Hussein, Fuzzy fractional shallow water wave equations: analysis, convergence of solutions, and comparative study with depth as triangular fuzzy number, *Physica Scripta*, Vol. 99, No. 12, pp. 125216, 2024.

[24] P. Karunakar, S. Chakraverty, Solution of interval shallow water wave equations using homotopy perturbation method, *Engineering Computations*, Vol. 35, No. 4, pp. 1610-1624, 2018.

[25] P. Karunakar, K. S. Reddy, S. Chakraverty, Stability analysis and approximate solution of interval mathematical model for the COVID-19 pandemic, *Mathematical Methods in the Applied Sciences*, 2023.

[26] P. Karunakar, U. Biswal, S. Chakraverty, Fluid dynamics problems in uncertain environment, *Mathematical methods in interdisciplinary sciences*, pp. 125-144, 2020.

[27] S. Chakraverty, N. Mahato, P. Karunakar, T. D. Rao, 2019, *Advanced numerical and semi-analytical methods for differential equations*, John Wiley & Sons,

[28] I. Podlubny, 1998, *Fractional differential equations: an introduction to fractional derivatives, fractional differential equations, to methods of their solution and some of their applications*, elsevier,

[29] M. R. Spiegel, 1965, *Laplace transforms*, McGraw-Hill New York,

[30] M. Madani, M. Fathizadeh, Y. Khan, A. Yildirim, On the coupling of the homotopy perturbation method and Laplace transformation, *Mathematical and Computer Modelling*, Vol. 53, No. 9-10, pp. 1937-1945, 2011.

[31] Y. Khan, Q. Wu, Homotopy perturbation transform method for nonlinear equations using He's polynomials, *Computers & Mathematics with Applications*, Vol. 61, No. 8, pp. 1963-1967, 2011.

[32] H. Aminikhah, The combined Laplace transform and new homotopy perturbation methods for stiff systems of ODEs, *Applied Mathematical Modelling*, Vol. 36, No. 8, pp. 3638-3644, 2012.

[33] A. Ghorbani, Beyond Adomian polynomials: he polynomials, *Chaos, Solitons & Fractals*, Vol. 39, No. 3, pp. 1486-1492, 2009.

[34] P. Karunakar, S. Chakraverty, Effect of Coriolis constant on Geophysical Korteweg-de Vries equation, *Journal of Ocean Engineering and Science*, Vol. 4, No. 2, pp. 113-121, 2019.